



MONTCLAIR STATE
UNIVERSITY

Montclair State University
**Montclair State University Digital
Commons**

Department of Chemistry and Biochemistry
Faculty Scholarship and Creative Works

Department of Chemistry and Biochemistry

2-1-2019

Single-Step Fabrication of Electrochemical Flow Cells Utilizing Multi-Material 3D Printing

Glen O'Neil

Montclair State University, oneilg@mail.montclair.edu

Shakir Ahmed

Montclair State University

Kevin Halloran

Montclair State University

Jordyn N. Janusz

Montclair State University

Alexandra Rodríguez

Montclair State University

See next page for additional authors

Follow this and additional works at: <https://digitalcommons.montclair.edu/chem-biochem-facpubs>

MSU Digital Commons Citation

O'Neil, Glen; Ahmed, Shakir; Halloran, Kevin; Janusz, Jordyn N.; Rodríguez, Alexandra; and Terrero Rodríguez, Irina M., "Single-Step Fabrication of Electrochemical Flow Cells Utilizing Multi-Material 3D Printing" (2019). *Department of Chemistry and Biochemistry Faculty Scholarship and Creative Works*. 4. <https://digitalcommons.montclair.edu/chem-biochem-facpubs/4>

This Article is brought to you for free and open access by the Department of Chemistry and Biochemistry at Montclair State University Digital Commons. It has been accepted for inclusion in Department of Chemistry and Biochemistry Faculty Scholarship and Creative Works by an authorized administrator of Montclair State University Digital Commons. For more information, please contact digitalcommons@montclair.edu.

Authors

Glen O'Neil, Shakir Ahmed, Kevin Halloran, Jordyn N. Janusz, Alexandra Rodríguez, and Irina M. Terrero Rodríguez



Full communication

Single-step fabrication of electrochemical flow cells utilizing multi-material 3D printing

Glen D. O'Neil*, Shakir Ahmed, Kevin Halloran, Jordyn N. Janusz, Alexandra Rodríguez, Irina M. Terrero Rodríguez

Department of Chemistry and Biochemistry, Montclair State University, Montclair, NJ 07043, United States of America

ARTICLE INFO

Keywords:

3D printing
Fused-deposition modeling
Additive manufacturing
Channel-flow electrode
Composite electrodes
3D printed electrode

ABSTRACT

Here we present methodology for fabricating electrochemical flow cells with embedded carbon-composite electrodes in a single step using simultaneous 3D printing of insulating poly(lactic acid) (PLA) and a commercially available graphene–PLA composite. This work is significant because it is the first demonstration that devices capable of fluid handling and electrochemical sensing can be produced in a single fabrication step using inexpensive equipment. We demonstrate the broad utility of this approach using a channel-flow configuration as an exemplary system for hydrodynamic electrochemistry. Unmodified devices were characterized using hydrodynamic electrochemistry, and behave according to the well-established Levich equation. We also characterized the fabrication reproducibility and found that the devices were within 3% RSD. The 3D-printed sensors we employed were subsequently modified by electroplating Au and used under flowing conditions to detect catechol, whose oxidation requires two electrons and two protons and is thus more challenging to analyze than the outer-sphere FcCH_2OH . We envision these results will pave the way for the development of highly customized micro-total analysis systems that include embedded electrochemical sensors for a variety of redox-active analytes.

1. Introduction

Sensors and devices incorporating 3D-printed components have gained significant attention recently [1–6]. 3D printable sensors have several features that make them attractive in a variety of fields: they are highly customizable [7]; devices can be produced in a number of unique and interesting geometries (e.g. solids containing internal voids) [8]; devices can be rapidly prototyped. As a result, there have been numerous applications of 3D printing in energy storage, sensors, and microfluidics [9–22].

For electroanalytical applications, 3D printing has been used for fabricating sensors for a variety of applications using conductive materials and for fabricating flow cells and microfluidic devices. Significant advances have been made in applying 3D printed metals and composites to a variety of chemical species including heavy metals and biological analytes [18–21,23–28]. 3D printing has also been widely used for the construction of hydrodynamic flow cells, which are used to increase mass transport of reactants to the electrode surface, thus increasing sensitivity and decreasing detection limits. One advantage of producing flow cells using 3D printing is the ability to rapidly produce

and test a wide variety of parameters that impact sensitivity (e.g., channel dimensions, inlet/outlet spacing, electrode placement) during the design phase. 3D printing has been used to produce channel-flow and wall-jet electrodes [8,29–32] that have shown promise for trace measurements of a variety of species [33–38].

Here, we demonstrate the ability to fabricate devices that incorporate both fluid handling and chemical sensors in a single fabrication step. We used an off-the-shelf commercial fused deposition modeling (FDM) 3D printer with dual extrusion capability to simultaneously print a PLA flow cell along with graphene–PLA composite electrodes embedded within (Fig. 1). We fabricate channel-flow electrochemical cells (CFEs) [39] and characterize their performance without modification or pretreatment using the fast outer-sphere redox couple ferrocene methanol. The electrodes were modified with electrodeposited Au, which we use to increase the sensitivity towards catechol.

* Corresponding author.

E-mail address: oneilg@montclair.edu (G.D. O'Neil).

<https://doi.org/10.1016/j.elecom.2018.12.006>

Received 16 November 2018; Received in revised form 3 December 2018; Accepted 12 December 2018

Available online 13 December 2018

1388-2481/ © 2018 The Authors. Published by Elsevier B.V. This is an open access article under the CC BY-NC-ND license (<http://creativecommons.org/licenses/by-nc-nd/4.0/>).

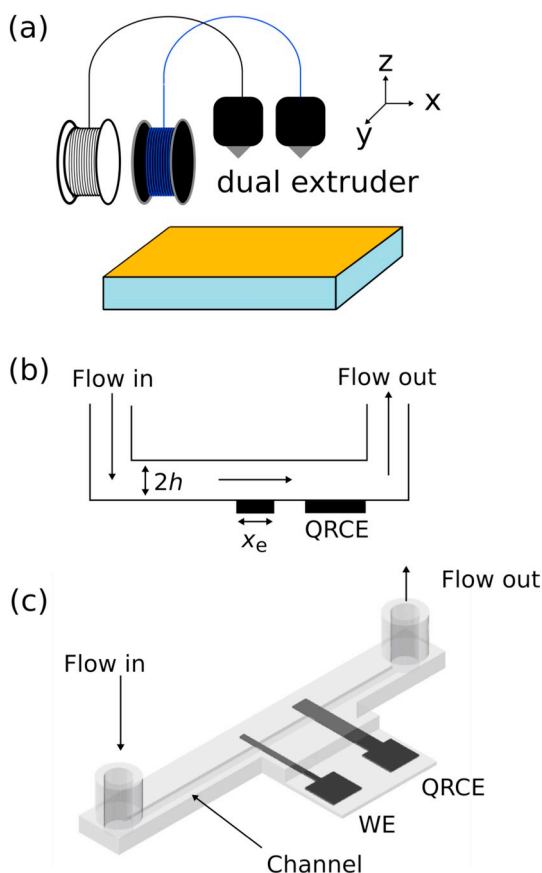


Fig. 1. Schematic of the experimental setup and devices. (a) schematic of dual extrusion 3D printing setup with two materials; (b) schematic representation of the channel flow geometry and the positions of the two electrodes. This schematic is not to scale; (c) CAD drawing of a channel flow cell with a $1.5 \text{ mm} \times 1.0 \text{ mm}$ channel and two band electrodes.

2. Experimental

2.1. Materials and solutions

Ferrocene methanol (FcCH_2OH ; 97%) was from Acros Organics, hydrogen tetrachloroaurate (III) trihydrate (99.99%) was from Alfa Aesar, and all other salts were from Fisher Scientific and were certified ACS grade and used as received. The clear poly(lactic acid) filament (PLA; 1.75 mm) was from MakerGear and the conductive graphene-PLA filament was purchased from BlackMagic3D. All solutions were prepared using $18.2 \text{ M}\Omega\cdot\text{cm}$ water (Millipore Simplicity).

2.2. 3D printing procedures

The flow cells and electrodes were designed separately using AutoDesk Inventor 2017 CAD software, and checked as an assembly to ensure all components fit together. The .stl files are available for download on our group website (gdolab.weebly.com). The CAD drawings were sliced for 3D printing using Simplify3D software with layer height: $100 \mu\text{m}$; extrusion width: 0.4 mm ; extrusion multiplier: 1.1; infill angle: $0^\circ/90^\circ$; infill percentage: 100%; infill extrusion width: 110%; extrusion temperature: 215°C ; bed temperature: 70°C ; print speed: 2400 mm min^{-1} [40]. The devices were printed by fused deposition modeling (FDM) using a MakerGear M2 Dual printer (Ohio, USA; Fig. 1a), which was modified with 0.35 mm stainless steel extruders (MakerGear) to reduce clogging from the carbon filament. The print bed was covered with Kapton tape to assist in adhesion of the 3D printed cells.

Besides the print settings listed above, there are several important experimental details which need to be considered during the 3D printing for high-quality, leak-free devices. Especially important are the distance between the extruder and the print bed, the alignment of the 3D printer bed to the extruder, and the adhesion of the first layer of print. We have established a set of pre-print checks that help improve print quality and reproducibility. First, the distance between the left filament extruder and print bed is set to be $100 \mu\text{m}$ using a feeler gauge and the alignment tool on MakerGear Quick Start software. For our printer, a $100 \mu\text{m}$ extruder-bed distance was critical for optimal extrusion width and for joining adjacent strands of polymer. Second, the print bed alignment was checked at the beginning of each day of printing, ensuring that the extruder-bed distance was constant for the entire bed surface. Third, the right extruder was aligned to the left extruder. We perform this by loosening the bolt holding the right extruder in place, so that it can move freely in the z-direction. We then carefully adjust the height of the bed in 0.01 mm increments until a feeler gauge will no longer move freely under the left extruder. We then secure the bolt holding the right extruder in place. Fourth, the print bed was sprayed with hairspray (Garnier Fructis Full Control Anti-Humidity) to ensure excellent adhesion for the first layer of print.

2.3. Electrochemical cell and measurements

A schematic of the channel-flow cell geometry is shown in Fig. 1b. All electrochemical experiments were performed at room temperature ($22 \pm 2^\circ\text{C}$) using a CHI 660E potentiostat (USA). Measurements within the flow cell were carried out in three-electrode mode with the thin band serving as the working electrode, a $\text{Ag}|\text{AgCl}$ pseudo-reference wire was placed in the outlet tubing, and the larger band was used as the counter unless otherwise noted.

3. Results and discussion

3.1. Device fabrication

Proof-of-concept devices consisted of a single 50 mm long channel with a cross-sectional dimension of $1.5 \times 1.0 \text{ mm}^2$ ($w \times 2h$; Fig. 1c). The versatility of 3D printing and fast device turnaround time mean that these parameters can be easily changed by modifying the CAD file and reprinting. Numerous devices were successfully printed and tested during development, however we only show data from $1.5 \times 1.0 \text{ mm}^2$ cells for manuscript clarity and consistency. The approach described herein is highly versatile and fast as new devices can be printed in $\sim 45 \text{ min}$, depending on print parameters, design complexity, and device size.

3.2. Electrochemical characterization of 3D printed flow cell

Hydrodynamic electrochemistry offers significantly higher mass transport rates than stationary measurements, which ultimately lead to increased sensitivity and decreased detection limits [8]. The channel flow configuration employed here employs a rectangular channel of variable dimensions that flows across inlaid band electrodes, which serve as the working and counter electrode (Fig. 1b). The CFE has been extensively modeled, enabling a convenient relationship between the limiting current and volumetric flow rate [41,42]:

$$i_{\text{lim}} = 0.925nF_c D^{2/3} V_f^{1/3} w^{2/3} h^{-2/3} x_e^{2/3} \quad (1)$$

where i_{lim} is the limiting current, V_f is the volumetric flow rate ($\text{cm}^3 \text{ s}^{-1}$), w is the channel width (cm), $2h$ is the channel height (cm), and x_e is the electrode width (cm), and n , F , c_b , and D have their usual meanings.

Fig. 2a shows linear sweep voltammograms (LSVs) collected for the oxidation of 1.4 mM FcCH_2OH in 0.4 M KCl for V_f over the range

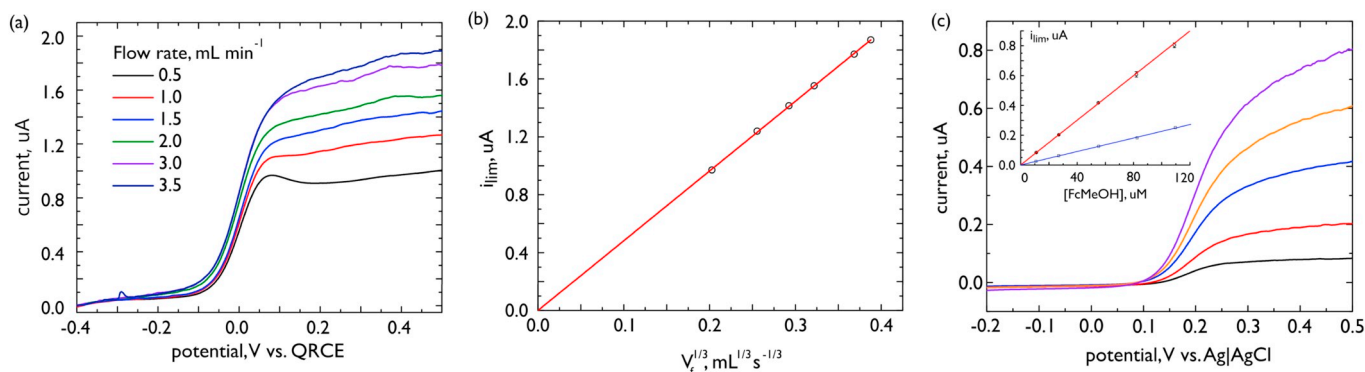


Fig. 2. Hydrodynamic voltammetry using a 3D printed flow cell. (a) LSVs of the oxidation of 1.4 mM FcCH₂OH in 0.4 M KCl. Wide band was used as the quasi-reference counter electrode; (b) effect of flow rate on the limiting current. (c) LSVs of FcCH₂OH over the concentration range 11–109 μM (1 M KCl as supporting electrolyte); inset shows the calibration plots for FcCH₂OH under flowing (red) and stagnant (blue) conditions. LSVs are an average of 4 independent measurements and error bars represent one standard deviation of the mean. Scan rate = 0.05 V s⁻¹. (For interpretation of the references to colour in this figure legend, the reader is referred to the web version of this article.)

0.5–3.5 mL min⁻¹. At 0.5 mL min⁻¹, the current reaches a peak at ~-0.05 V vs. QRCE before leveling off. At these low flow rates, both diffusion and convection influence the response of the electrode. For flow rates of ~1.0 mL min⁻¹ and above, the current approaches a limiting value, although there is some drift in the measured current in the anodic scan. It is possible that the current drift is caused by surface roughness of the 3D-printed electrode/channel walls or small gaps/divots where the insulating channel meets the conductive electrode. A plot of i_{lim} versus $V_f^{1/3}$ shows excellent linearity ($R^2 = 0.9999$; Fig. 2b), consistent with the convective transport expected in channel-flow electrochemical cells. However, the gradient of the best-fit line ($4.82(\pm 0.01) \mu\text{A s}^{-1/3} \text{ mL}^{-1/3}$) deviates significantly from the expected value calculated using Eq. (1) ($19.0 \mu\text{A s}^{-1/3} \text{ mL}^{-1/3}$), suggesting that there are significant deviations to channel and/or electrode dimensions compared to the CAD design. The theoretical slope was calculated using Eq. (1) with the following values: $n = 1$, $F = 96,485 \text{ C mol}^{-1}$, $c_b = 1.4 \cdot 10^{-6} \text{ mol cm}^{-3}$, $D = 7.80 \cdot 10^{-6} \text{ cm}^2 \text{ s}^{-1}$ [43], $w = 0.15 \text{ cm}$, $h = 0.05 \text{ cm}$, $x_e = 0.08 \text{ cm}$.

As an initial demonstration that these simple, low-cost devices can be used for quantitative analysis of freely diffusing redox species, we performed linear sweep voltammetry in flowing and stagnant solutions of FcCH₂OH. Fig. 2c shows averaged LSVs ($n = 4$) collected at 3.0 mL min⁻¹ for solutions of FcCH₂OH. At each concentration, a near steady-state response is observed at 0.5 V vs. Ag|AgCl. Note that the 3D printed electrodes were not modified in any way prior to these experiments. The inset to Fig. 2c shows a plot of i_{lim} versus FcCH₂OH concentration and displays excellent linearity ($R^2 = 0.9998$), as expected. The sensitivity under hydrodynamic conditions was $7.48(\pm 0.06) \times 10^{-3} \mu\text{A } \mu\text{M}^{-1}$, which is ~3.4 times higher than the sensitivity observed under stationary conditions (blue trace, Fig. 2c inset), highlighting the advantage of the fast mass transport rates achievable using this simple device.

We characterized the print-to-print reproducibility of the flow cells by printing three devices and characterizing their electrochemical behavior using stagnant CVs of FcCH₂OH (Fig. 3a). Any significant changes in device geometry or electrode quality should impact the peak current. The average peak current of the CVs was $0.72(\pm 0.02) \mu\text{A}$, which shows that the devices are remarkably reproducible with a 3% relative standard deviation. We also characterized the cycling stability of the carbon electrodes by performing CVs in FcCH₂OH for 25 cycles (Fig. 3b). The anodic peak current initially increases ~50 nA over the first 5 cycles, after which the peak current is stable (Fig. 3c). The peak current was remarkably consistent, with < 0.1% relative standard deviation, suggesting that no parasitic side reactions or fouling occurred on the surface of the electrode over this time frame.

3.3. Electrochemical detection of catechol in the 3D printed flow cells

In order to demonstrate that these devices can be used for more complex electrochemical reactions, we measured catechol (Fig. 4a, inset) in artificial cerebral spinal fluid (aCSF) buffer under flowing conditions. Catechol undergoes a two-electron, two-proton oxidation to form *o*-quinone [44–46] and is thus a more challenging molecule to analyze than FcCH₂OH. In order to improve the electrochemical behavior of the 3D-printed electrodes, we first electrodeposited a thin layer of Au from a 1 mM solution of HAuCl₄ with 0.1 M HCl as the supporting electrolyte. Electrodeposited Au has recently been shown to improve the electron transfer behavior of carbon fiber microelectrodes towards dopamine [47]. Fig. 4a shows background-subtracted, averaged LSVs ($n = 5$) collected at 3.0 mL min⁻¹ for solutions of catechol. The voltammograms are quasi-sigmoidal, but reach limiting currents at potentials > 0.6 V. Fig. 4b shows a calibration plot of the limiting current at 0.6 V vs. Ag|AgCl as a function of catechol concentration. The calibration curve displays excellent linearity ($R^2 = 0.9997$) with a gradient of $0.0208(\pm 0.0002) \mu\text{A } \mu\text{M}^{-1}$. The limit of detection ($\text{LOD} = 3\sigma_{/m}$) for catechol was 1.4 μM.

4. Summary and conclusions

Here, we have presented a simple, fast, and inexpensive method for preparing 3D-printed electrochemical flow cells in a single step. The practical use of this methodology is that it greatly simplifies the fabrication of devices incorporating (potentially) complex fluid handling with electrochemical detection. We employed the fast, one-electron oxidation of FcCH₂OH to characterize the unmodified cells under stagnant and hydrodynamic conditions, and demonstrated quantitative measurements of FcCH₂OH and catechol (after modification of the electrodes with electrodeposited Au) as exemplary species. Because these devices are highly customizable and easily optimized by iterative design, we expect them to be useful for a variety of analyses and for investigating novel flow-cell configurations and electrode geometries.

Although these results demonstrate that 3D printable sensors can be integrated with complex fluid handling, there is considerable scope for improvement with the aim of tackling more challenging electro-analytical problems. First, we expect that the observed detection limits would be improved by increasing the flow rate, optimizing the cell geometry (e.g., decreasing the channel height and using a wider channel), employing a nonlinear potential waveform (e.g., differential pulse), or using flow-injection analysis. Second, the results obtained in flowing solutions did not reach a true steady state, which suggests there is significant roughness inside the channel. This has been previously

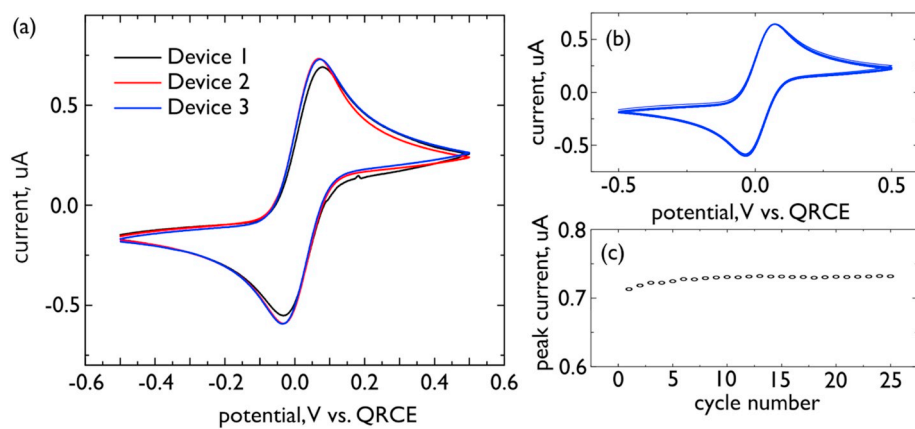


Fig. 3. 3D-printed flow cells with embedded carbon electrodes are reproducible. (a) CVs of 1.4 mM FcCH₂OH in 0.4 M KCl using three independently printed devices. (b) 25 consecutive CVs measured in 1.4 mM FcCH₂OH with 0.4 M KCl as the supporting electrolyte; (c) plot of anodic peak current as a function of cycle number. Scan rate = 0.05 V s⁻¹. (For interpretation of the references to colour in this figure legend, the reader is referred to the web version of this article.)

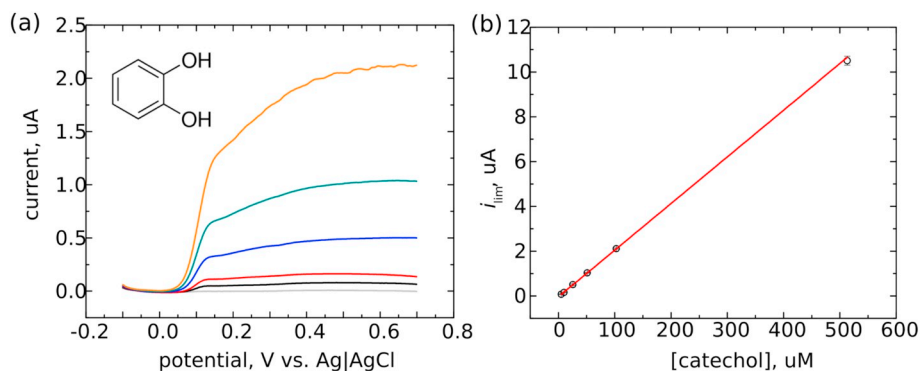


Fig. 4. Detection of catechol in aCSF inside a monolithic 3D-printed flow cell. (a) LSVs of catechol over the concentration range 5.1–103 μM; scan rate = 0.05 V s⁻¹; (b) calibration plot showing a linear regression of the limiting current data from (a). LSVs are background-subtracted and presented as the average of 5 independent measurements; error bars represent one standard deviation. Scan rate = 0.05 V s⁻¹; V_f = 3.0 mL min⁻¹. (For interpretation of the references to colour in this figure legend, the reader is referred to the web version of this article.)

observed by other groups in 3D printed microfluidics made using FDM [48–50]. We also suspect the interface between the insulating and conductive materials is not perfectly coplanar, which will also lead to deviations from theory. The channels presented herein were relatively large (1.5 mm × 1.0 mm) and we expect that imperfections inside the channel would cause even more significant deviation from theory as the dimensions of the channel shrink towards true microfluidic dimensions. This is significant because detection limits can be improved by decreasing the channel dimensions, and the roughness of the channels places a constraint on achievable channel dimensions. Nevertheless, many practical applications do not require channels of true microfluidic dimensions [7]. Third, while the current response of the flow cells behaved according to the Levich equation for a channel-flow geometry (Fig. 2b), the measured currents did not agree with those predicted using Eq. (1). This strongly implies that the printed channel dimensions do not agree with those defined in the CAD file.

We also expect improvements to be made in the performance of the composite material used for the electrodes in these devices. In separate experiments (data not shown), we observed that polishing the 3D-printed filament with sandpaper and alumina slurries significantly improved the electrochemical response towards outer-sphere redox couples. This observation is fairly common using composite electrodes and was recently shown by Henry et al. to drastically improve the performance of thermoplastic electrodes made with carbon and poly(methyl methacrylate) [51]. As a result, we expect polishing the electrodes inside the channel may lead to improved responses. Alternatively, there are chemical approaches to improving the response of the graphene-PLA electrodes. For instance, Pumera et al. used dimethylformamide (DMF) to dissolve the electrochemically inactive polymeric binder of BlackMagic 3D and expose more electrochemically active carbon nanostructures, which improved the electrochemical behavior [20,52]. We expect that further detailed investigations of the surface/interface properties of 3D printable carbon electrodes will yield more sensitive (and potentially selective) electrochemical performance of this 3D

printable composite material in the future.

Acknowledgements

This work was supported by funds provided by Montclair State University. JNJ acknowledges the Science Honors Innovation Program (SHIP) at Montclair State for financial support. ITR acknowledges support from Dominican Republic's Ministry of Higher Education, Science and Technology. We thank Julie Macpherson for helpful discussions.

References

- [1] A. Ambrosi, M. Pumera, 3D-printing technologies for electrochemical applications, *Chem. Soc. Rev.* 45 (2016) 2740–2755, <https://doi.org/10.1039/c5cs00714c>.
- [2] C.L. Manzanera Palenzuela, M. Pumera, (Bio)analytical chemistry enabled by 3D printing: sensors and biosensors, *TrAC Trends Anal. Chem.* 103 (2018) 110–118, <https://doi.org/10.1016/j.trac.2018.03.016>.
- [3] H.H. Hamzah, S.A. Shafiee, A. Abdalla, B.A. Patel, 3D printable conductive materials for the fabrication of electrochemical sensors: a mini review, *Electrochem. Commun.* 96 (2018) 27–31, <https://doi.org/10.1016/j.elecom.2018.09.006>.
- [4] B.C. Gross, S.Y. Lockwood, D.M. Spence, Recent advances in analytical chemistry by 3D printing, *Anal. Chem.* 89 (2017) 57–70, <https://doi.org/10.1021/acs.analchem.6b04344>.
- [5] J. Lee, J. An, C.K. Chua, Fundamentals and applications of 3D printing for novel materials, *Appl. Mater. Today* 7 (2017) 120–133, <https://doi.org/10.1016/j.apmt.2017.02.004>.
- [6] S.W. Kwok, K.H.H. Goh, Z.D. Tan, S.T.M. Tan, W.W. Tjiu, J.Y. Soh, Z.J.G. Ng, Y.Z. Chan, H.K. Hui, K.E.J. Goh, Electrically conductive filament for 3D-printed circuits and sensors, *Appl. Mater. Today* 9 (2017) 167–175, <https://doi.org/10.1016/j.apmt.2017.07.001>.
- [7] J.F. Rusling, Developing microfluidic sensing devices using 3-D printing, *ACS Sensors* (3) (2018) 522–526, <https://doi.org/10.1021/acssensors.8b00079>.
- [8] R.B. Channon, M.B. Joseph, J.V. Macpherson, Additive manufacturing for electrochemical (micro)fluidic platforms, *Electrochem. Soc. Interface* 25 (2016) 63–68.
- [9] G.D. O'Neil, C.D. Christian, D.E. Brown, D.V. Esposito, Hydrogen production with a simple and scalable membraneless electrolyzer, *J. Electrochem. Soc.* 163 (2016) F3012–F3019, <https://doi.org/10.1149/2.0021611jes>.
- [10] O.O. Talabi, A.E. Dorfi, G.D. O'Neil, D.V. Esposito, Membraneless electrolyzers for the simultaneous production of acid and base, *Chem. Commun.* 53 (2017)

- 8006–8009, <https://doi.org/10.1039/C7CC02361H>.
- [11] Y. He, Y. Wu, J. Fu, Q. Gao, J. Qiu, Developments of 3D printing microfluidics and applications in chemistry and biology: a review, *Electroanalysis* 28 (2016) 1658–1678, <https://doi.org/10.1002/elan.201600043>.
- [12] A.A. Yazdi, A. Popma, W. Wong, T. Nguyen, Y. Pan, J. Xu, 3D printing: an emerging tool for novel microfluidics and lab-on-a-chip applications, *Microfluid. Nanofluid.* 20 (2016) 50, <https://doi.org/10.1007/s10404-016-1715-4>.
- [13] N. Bhattacharjee, A. Urrios, S. Kang, A. Folch, The upcoming 3D-printing revolution in microfluidics, *Lab Chip* 16 (2016) 1720–1742, <https://doi.org/10.1039/C6LC001426G>.
- [14] A. Ambrosi, M. Pumera, Multimaterial 3D-printed water electrolyzer with earth-abundant electrodeposited catalysts, *ACS Sustain. Chem. Eng.* 6 (2018) 16968–16975, <https://doi.org/10.1021/acsschemeng.8b04327>.
- [15] J.T. Davis, J. Qi, X. Fan, J.C. Bui, D.V. Esposito, Floating membraneless PV-electrolyzer based on buoyancy-driven product separation, *Int. J. Hydrog. Energy* 43 (2018) 1224–1238, <https://doi.org/10.1016/j.ijhydene.2017.11.086>.
- [16] G. Chisholm, P.J. Kitson, N.D. Kirkaldy, L.G. Bloor, L. Cronin, 3D printed flow plates for the electrolysis of water: an economic and adaptable approach to device manufacture, *Energy Environ. Sci.* 7 (2014) 3026–3032, <https://doi.org/10.1039/C4EE01426J>.
- [17] C. Parra-Cabrera, C. Achille, S. Kuhn, R. Ameloot, 3D printing in chemical engineering and catalytic technology: structured catalysts, mixers and reactors, *Chem. Soc. Rev.* 47 (2017) 209–230, <https://doi.org/10.1039/C7CS00631D>.
- [18] C. Tan, M. Za, M. Nasir, A. Ambrosi, M. Pumera, 3D printed electrodes for detection of nitroaromatic explosives and nerve agents, *Anal. Chem.* 89 (2017) 8995–9001, <https://doi.org/10.1021/acs.analchem.7b01614>.
- [19] E.H.Z. Ho, A. Ambrosi, M. Pumera, Additive manufacturing of electrochemical interferences: simultaneous detection of biomarkers, *Appl. Mater. Today* 12 (2018) 43–50, <https://doi.org/10.1016/j.apmt.2018.03.008>.
- [20] C.L.M. Palenzuela, F. Novotny, P. Krupic, Z. Sofer, M. Pumera, 3D-printed graphene/polyactic acid electrodes promise high sensitivity in electroanalysis, *Anal. Chem.* 90 (2018) 5753–5759, <https://doi.org/10.1021/acs.analchem.8b00083>.
- [21] K.Y. Lee, A. Ambrosi, M. Pumera, 3D-printed metal electrodes for heavy metals detection by anodic stripping voltammetry, *Electroanalysis* 29 (2017) 2444–2453, <https://doi.org/10.1002/elan.201700388>.
- [22] A.K. Au, W. Huynh, L.F. Horowitz, A. Folch, 3D-printed microfluidics, *Angew. Chem. Int. Ed.* 55 (2016) 3862–3881, <https://doi.org/10.1002/anie.201504382>.
- [23] A. Ambrosi, J. Guo, S. Moo, M. Pumera, Helical 3D-printed metal electrodes as custom-shaped 3D platform for electrochemical devices, *Adv. Funct. Mater.* 26 (2016) 698–703, <https://doi.org/10.1002/adfm.201503902>.
- [24] B.R. Liyarita, A. Ambrosi, M. Pumera, 3D-printed electrodes for sensing of biologically active molecules, *Electroanalysis* 30 (2018) 1319–1326, <https://doi.org/10.1002/elan.201700828>.
- [25] Z. Rymansaib, P. Irvani, E. Emslie, M. Medvidović-Kosanović, M. Sak-Bosnar, R. Verdejo, F. Marken, All-polystyrene 3D-printed electrochemical device with embedded carbon nanofiber-graphite-polystyrene composite conductor, *Electroanalysis* 28 (2016) 1517–1523, <https://doi.org/10.1002/elan.201600017>.
- [26] K.C. Honeychurch, Z. Rymansaib, P. Irvani, Anodic stripping voltammetric determination of zinc at a 3-D printed carbon nanofiber–graphite–polystyrene electrode using a carbon pseudo-reference electrode, *Sensors Actuators B Chem.* 267 (2018) 476–482, <https://doi.org/10.1016/j.snb.2018.04.054>.
- [27] H.H. Bin Hamzah, O. Keattch, D. Covill, B.A. Patel, The effects of printing orientation on the electrochemical behaviour of 3D printed acrylonitrile butadiene styrene (ABS)/carbon black electrodes, *Sci. Rep.* 8 (2018) 9135, <https://doi.org/10.1038/s41598-018-27188-5>.
- [28] C.W. Foster, M.P. Down, Z. Yan, X. Ji, S.J. Rowley-Neale, G.C. Smith, P.J. Kelly, C.E. Banks, 3D printed graphene based energy storage devices, *Sci. Rep.* 7 (2017) 42233, <https://doi.org/10.1038/srep42233>.
- [29] M.J. Kimlinger, R.S. Martin, The use of a 3D-printed microfluidic device and pressure mobilization for integrating capillary electrophoresis with electrochemical detection, *Electroanalysis* 30 (2018) 2441–2449, <https://doi.org/10.1002/elan.201800367>.
- [30] A.S. Munshi, R.S. Martin, Microchip-based electrochemical detection using a 3-D printed wall-jet electrode device, *Analyst* 141 (2015) 862–869, <https://doi.org/10.1039/c5an01956g>.
- [31] M.E. Snowden, P.H. King, J.A. Covington, J.V. Macpherson, P.R. Unwin, Fabrication of versatile channel flow cells for quantitative electroanalysis using prototyping, *Anal. Chem.* 82 (2010) 3124–3131, <https://doi.org/10.1021/ac100345v>.
- [32] J.L. Erkal, A. Selimovic, B.C. Gross, S.Y. Lockwood, E.L. Walton, S. McNamara, R.S. Martin, D.M. Spence, 3D printed microfluidic devices with integrated versatile and reusable electrodes, *Lab Chip* 14 (2014) 2023–2032, <https://doi.org/10.1039/c4lc00171k>.
- [33] S. Sansuk, E. Bitziou, M.B. Joseph, J.A. Covington, M.G. Boutelle, P.R. Unwin, J.V. MacPherson, Ultrasensitive detection of dopamine using a carbon nanotube network microfluidic flow electrode, *Anal. Chem.* 85 (2013) 163–169, <https://doi.org/10.1021/ac3023586>.
- [34] R.B. Channon, M.B. Joseph, E. Bitziou, A.W.T. Bristow, A.D. Ray, J.V. Macpherson, Electrochemical flow injection analysis of hydrazine in an excess of an active pharmaceutical ingredient: achieving pharmaceutical detection limits electrochemically, *Anal. Chem.* 87 (2015) 10064–10071, <https://doi.org/10.1021/acs.analchem.5b02719>.
- [35] E. Bitziou, M.B. Joseph, T.L. Read, N. Palmer, T. Mollart, M.E. Newton, J.V. Macpherson, In situ optimization of pH for parts-per-billion electrochemical detection of dissolved hydrogen sulfide using boron doped diamond flow electrodes, *Anal. Chem.* 86 (2014) 10834–10840.
- [36] K. Kadimisetty, S. Malla, K.S. Bhalerao, I.M. Mosa, S. Bhakta, N.H. Lee, J.F. Rusling, Automated 3D-printed microfluidic array for rapid nanomaterial-enhanced detection of multiple proteins, *Anal. Chem.* 90 (2018) 7569–7577, <https://doi.org/10.1021/acs.analchem.8b01198>.
- [37] G.W. Bishop, J.E. Satterwhite-Warden, I. Bist, E. Chen, J.F. Rusling, Electrochemiluminescence at bare and DNA-coated graphite electrodes in 3D-printed fluidic devices, *ACS Sensors* 1 (2016) 197–202, <https://doi.org/10.1021/acssensors.5b00156>.
- [38] K. Kadimisetty, A.P. Spak, K.S. Bhalerao, M. Sharafeldin, I.M. Mosa, N.H. Lee, J.F. Rusling, Automated 4-sample protein immunoassays using 3D-printed microfluidics, *Anal. Methods* 10 (2018) 4000–4006, <https://doi.org/10.1039/C8AY01271G>.
- [39] J.A. Cooper, R.G. Compton, Channel electrodes - a review, *Electroanalysis* 10 (1998) 141–155, [https://doi.org/10.1002/\(SICI\)1521-4109\(199803\)10:3<141::AID-ELAN141>3.0.CO;2-F](https://doi.org/10.1002/(SICI)1521-4109(199803)10:3<141::AID-ELAN141>3.0.CO;2-F).
- [40] A.J.L. Morgan, L.H. San Jose, W.D. Jamieson, M. Wymant, B. Song, P. Stephens, D.A. Barrow, O.K. Castell, Simple and versatile 3D printed microfluidics using fused filament fabrication, *PLoS One* 11 (2016) e0152023, <https://doi.org/10.1371/journal.pone.0152023>.
- [41] V.G. Levich, *Physicochemical Hydrodynamics*, Prentice Hall, Englewood Cliffs, NJ, 1962.
- [42] R.G. Compton, P.R. Unwin, Channel and tubular electrodes, *J. Electroanal. Chem.* 205 (1986) 1–20.
- [43] J.H. Park, S.-N. Thorgaard, B. Zhang, A.J. Bard, Single particle detection by area amplification: single wall carbon nanotube attachment to a nanoelectrode, *J. Am. Chem. Soc.* 135 (2013) 5258–5261.
- [44] D.L. Robinson, A. Hermans, A.T. Seipel, R.M. Wightman, Monitoring rapid chemical communication in the brain, *Chem. Rev.* 108 (2008) 2554–2584, <https://doi.org/10.1021/cr068081q>.
- [45] R.A. Saraceno, A.G. Ewing, Electron transfer reactions of catechols at ultrasmall carbon ring electrodes, *Anal. Chem.* 60 (1988) 2016–2020, <https://doi.org/10.1021/ac00170a006>.
- [46] B. Wolfrum, M. Zevenbergen, S. Lemay, Nanofluidic redox cycling amplification for the selective detection of catechol, *Anal. Chem.* 80 (2008) 972–977, <https://doi.org/10.1021/ac7016647>.
- [47] S. Barlow, M. Louie, R. Hao, P. Defnet, B. Zhang, Electrodeposited gold on carbon-fiber microelectrodes enhances amperometric detection of dopamine release from pheochromocytoma cells, *Anal. Chem.* 90 (2018) 10049–10055, <https://doi.org/10.1021/acs.analchem.8b02750>.
- [48] G.I.J. Salentijn, P.E. Oomen, M. Grajewski, E. Verpoorte, Fused deposition modeling 3D printing for (bio)analytical device fabrication: procedures, materials, and applications, *Anal. Chem.* 89 (2017) 7053–7061, <https://doi.org/10.1021/acs.analchem.7b00828>.
- [49] F. Li, N.P. Macdonald, R.M. Guijt, M.C. Breadmore, Using printing orientation for tuning fluidic behavior in microfluidic chips made by fused deposition modeling 3D printing, *Anal. Chem.* 89 (2017) 12805–12811, <https://doi.org/10.1021/acs.analchem.7b03228>.
- [50] N.P. Macdonald, J.M. Cabot, P. Smejkal, R.M. Guijt, B. Paull, M.C. Breadmore, Comparing microfluidic performance of three-dimensional (3D) printing platforms, *Anal. Chem.* 89 (2017) 3858–3866, <https://doi.org/10.1021/acs.analchem.7b00136>.
- [51] K.J. Klunder, Z. Nilsson, J.B. Sambur, C.S. Henry, Patternable solvent-processed thermoplastic graphite electrodes, *J. Am. Chem. Soc.* 139 (2017) 12623–12631, <https://doi.org/10.1021/jacs.7b06173>.
- [52] M.P. Browne, F. Novotný, Z. Sofer, M. Pumera, 3D printed graphene electrodes' electrochemical activation, *ACS Appl. Mater. Interfaces* 10 (2018) 40294–40301, <https://doi.org/10.1021/acsami.8b14701>.